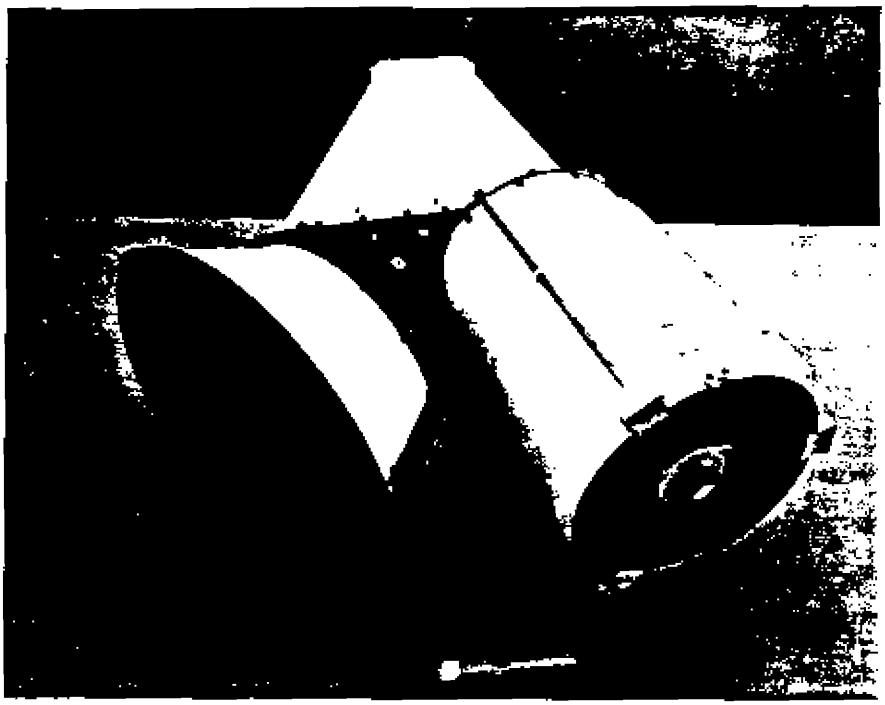

Fig. 1. Photograph of the NIMS Instrument.

The telescope is shown on the right, with one of the athermalizing Invar rods, separating the primary and secondary mirrors, visible outside the telescope housing. The spectrometer portion is at the rear, while the radiative cooler is facing at the left. The black portion at the center of the cooler is the radiating surface. This is surrounded by a shield which obscures radiation from the scan platform and much of the spacecraft.

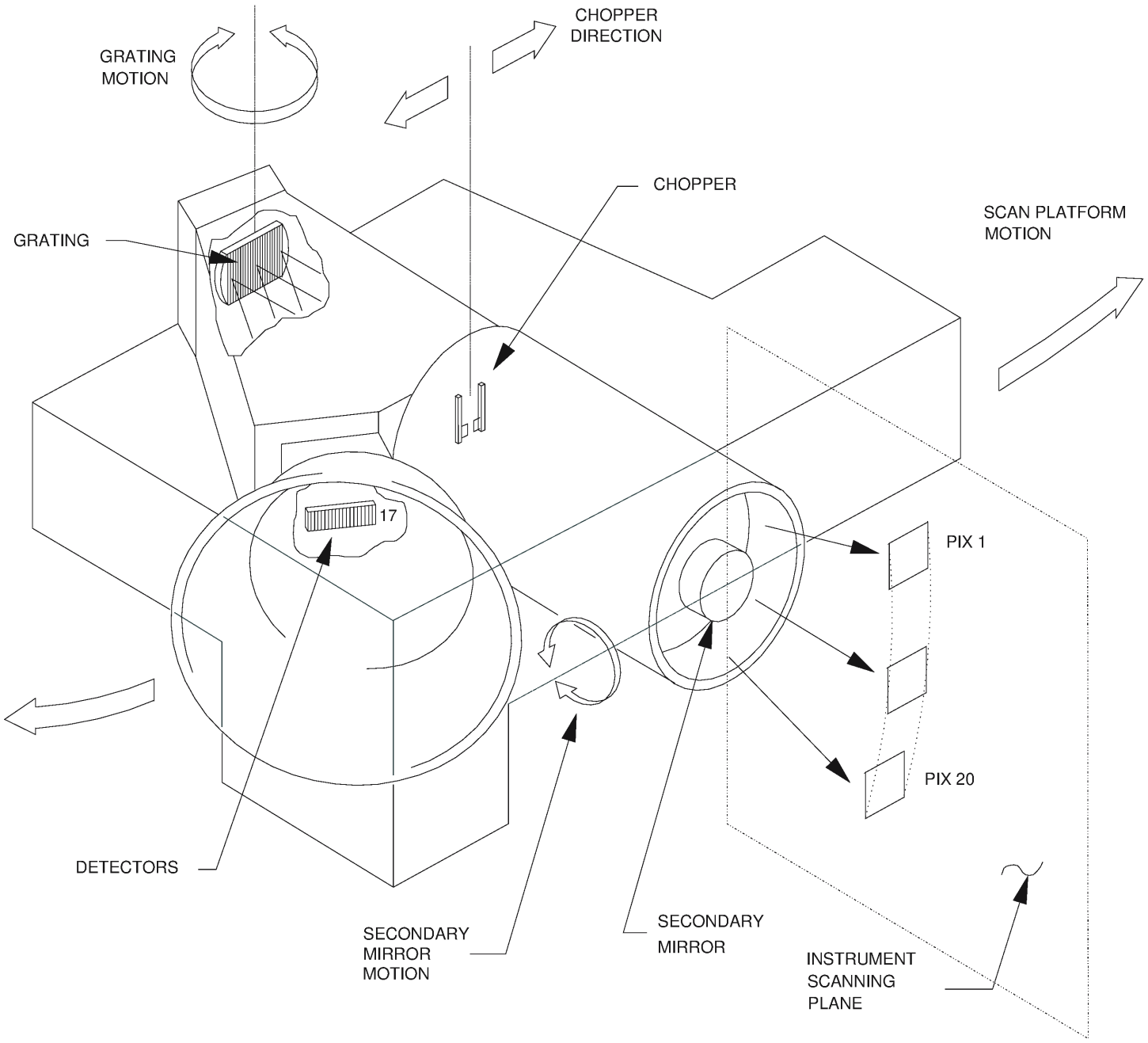

Fig. 2. Schematic Diagram of the Instrument and Scanning Motions.

The instrument is shown as it would appear sitting in the spacecraft scan platform. The cone angle motion of the scan platform is illustrated by the large arrows. The internal 20-position spatial scan, produced by motion of the telescope secondary mirror, is in the orthogonal cross-cone direction. The position of the initial pixel in a major frame (RIM) is shown as pixel 1. The plane of spectral dispersion is parallel to the plane of cone angle motion.

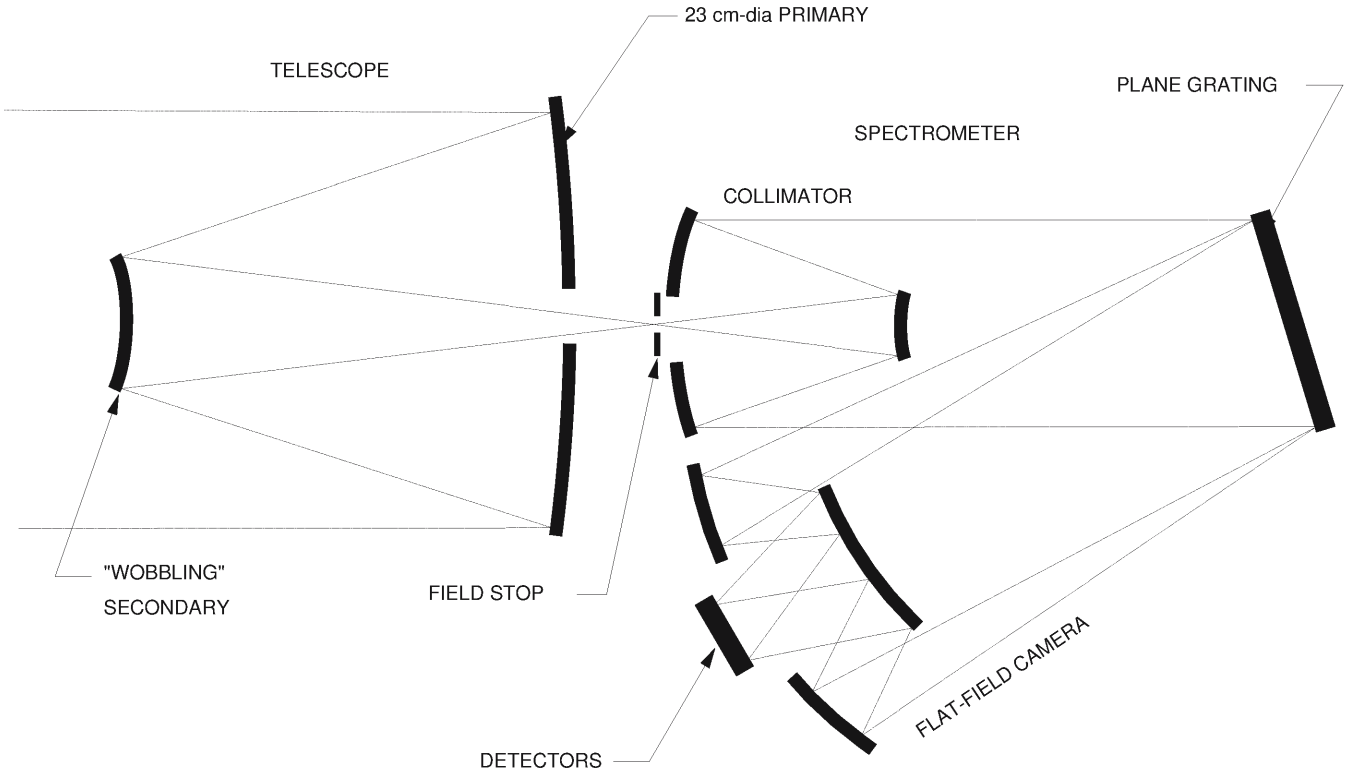

Fig. 3. Schematic of the NIMS Optical Design.

A telescope of 228 mm aperture forms an image at the entrance slit of the spectrometer. The telescope secondary mirror pivots around an axis which is in the plane of the paper, giving a 20-position spatial scan. The spectrometer employs a dual-blazed diffraction grating. The dispersed radiation is detected by 17 detectors in the camera focal plane, each detector located for a particular spectral region. Rotation of the grating changes the wavelength striking each detector. A complete spectrum, at full spectral resolution, is accomplished with 24 grating positions.

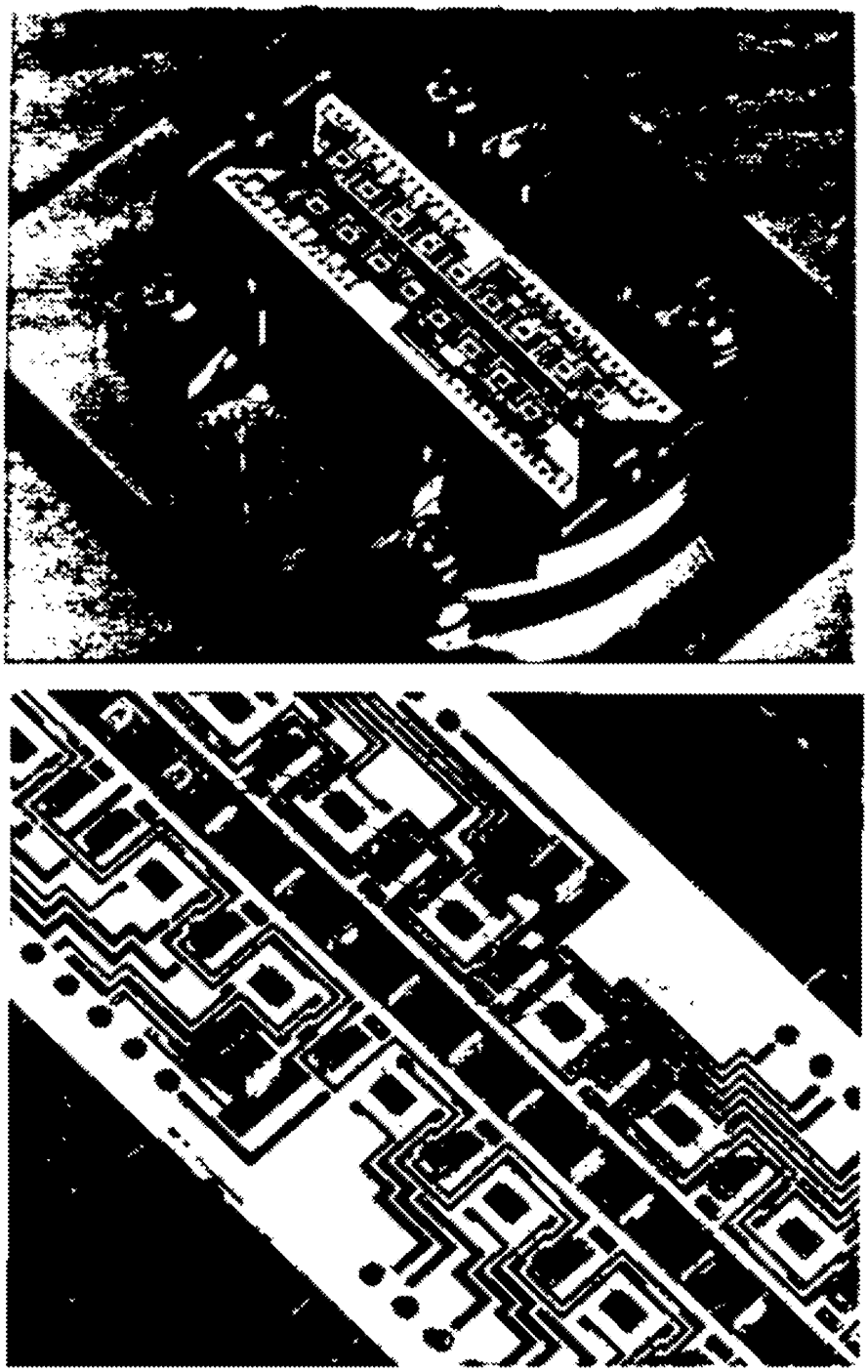

Fig. 4. Photographs of the Focal Plane Assembly.

This photograph shows the lower portion of the tantalum case and the wire-bonded hybrid circuitry containing the detectors, dual field effect transistors, feedback resistors, and decoupling capacitors. Not shown are the spectral blocking filters, field-of-view limiters, and the upperportion of the tantalum case containing the sapphire optical input window. The completed unit is evacuated and hermitically sealed using an indium gasket.

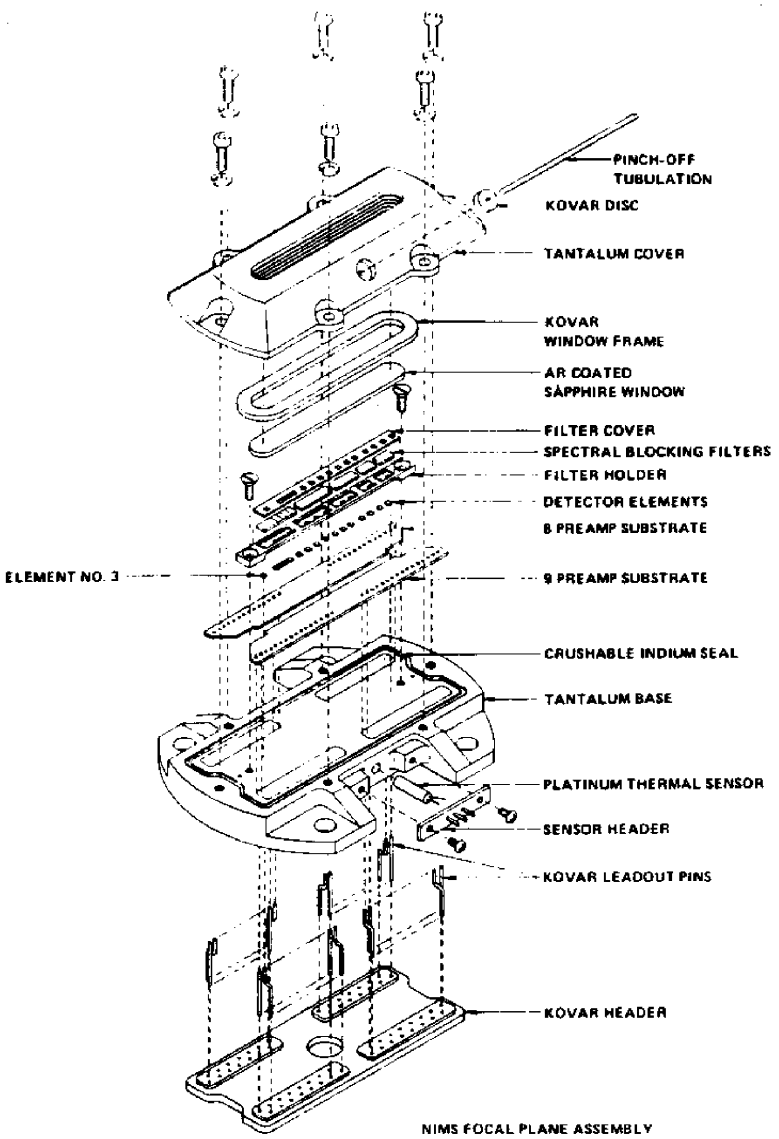

Fig. 5. Focal Plane Assembly Components.

The Focal Plane Assembly (FPA) contains seventeen individual photovoltaic diodes (15 InSb, 2 Si) and their associated preamplifier components, optical filters, field limiters, an optical window, a sealed Ta housing, a Pt temperature sensor, and feed-through connectors which couple to a low thermal conductivity ribbon cable (not shown).

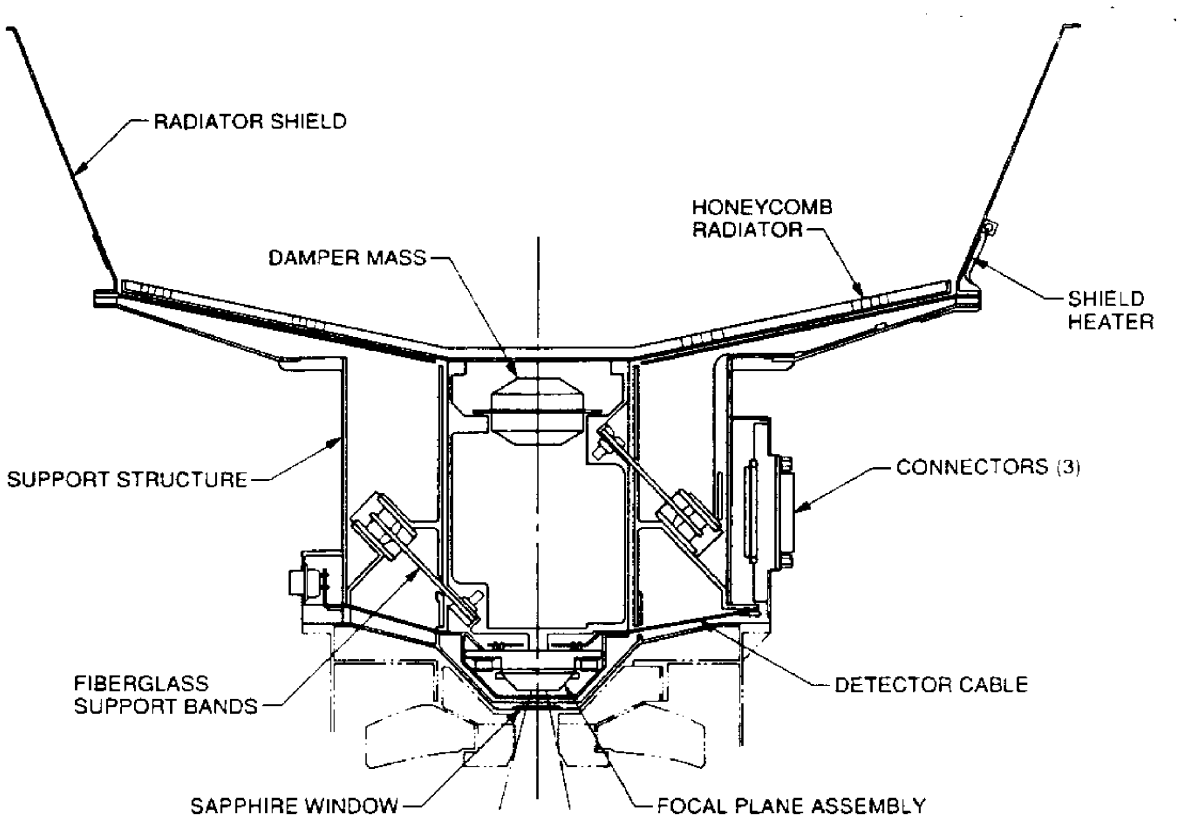

Fig. 6. Radiative Cooler Assembly.

The Focal Plane Assembly (FPA) is thermally coupled to a honeycomb radiator. Operating temperatures of 64 kelvins are achieved by radiation and by minimizing thermal loads to the FPA-radiator stage through use of low thermal conductivity fiberglass support bands and low emittance surfaces. A shield surrounds the radiator plate to block thermal emission from the scan platform and other portions of the spacecraft. The shield can be heated to 300 kelvins in order to avoid contamination of the low-emissivity inner surface of the shield. The outer surface, on the side facing away from the scan platform, is painted with high-emissivity paint to allow the shield to radiatively cool, while the surface facing the platform is thermally blanketed to reduce scan platform radiative loads to the shield. The outer diameter of the shield periphery is ~ 40 cm.

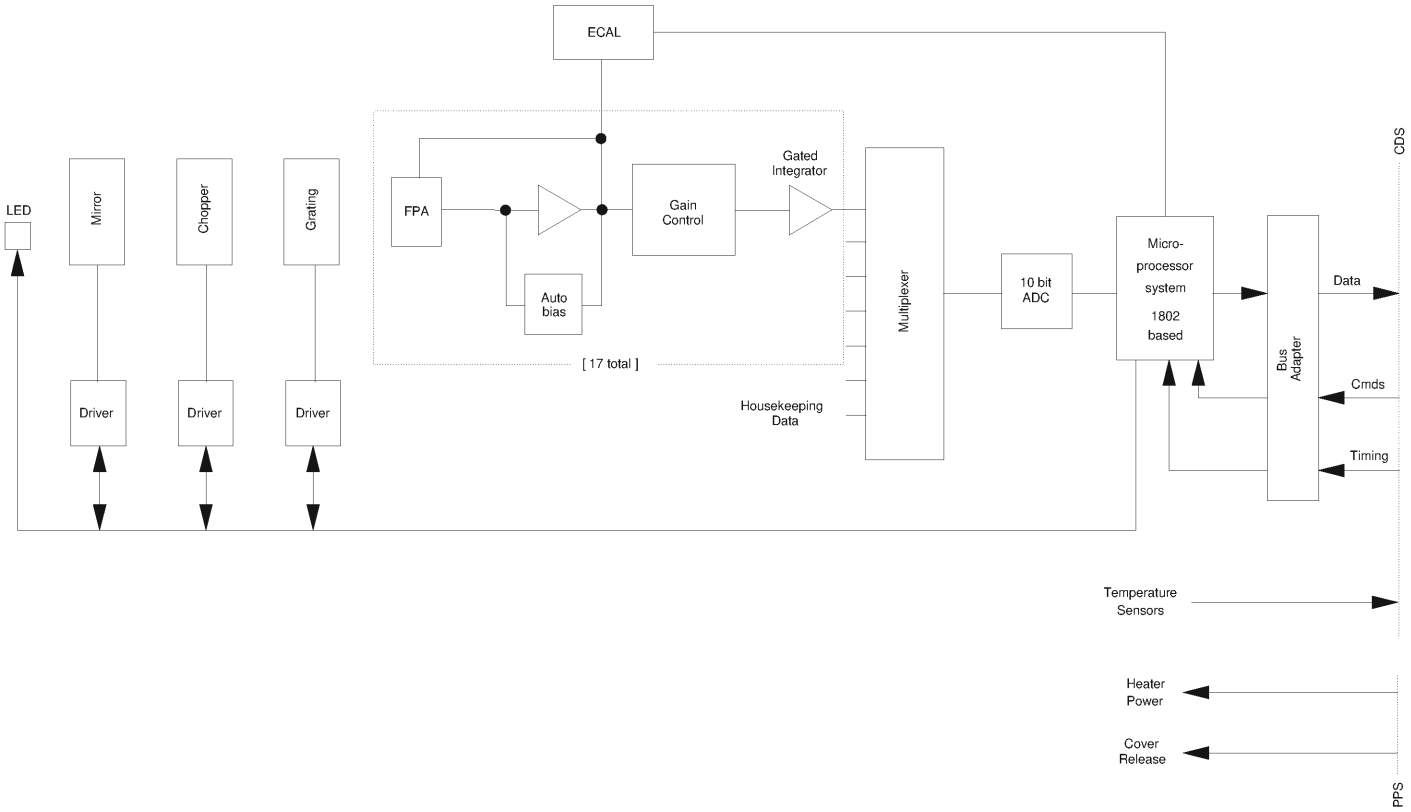

Fig. 7. Electronics Block Diagram.

The instrument is controlled by an 1802 microprocesser which communicates with the spacecraft Command and Data Subsystem (CDS) through a bus adaptor. The microprocesser controls the mirror, grating, and chopper mechanisms, the timing of the signal chains, and calibration and housekeeping measurements. There are individual signal chains for each detector, and their outputs are sampled with an analog multiplexer and digitized to 10 bit precision. There are six temperatures monitored within the instrument (telescope, chopper, spectrometer, radiator shield, focal plane, and electronics). These measurements are obtained directly by the CDS. Heater and cover release functions are performed by commandable functions in the Power and Pyrotechnic Subsystems (PPS).

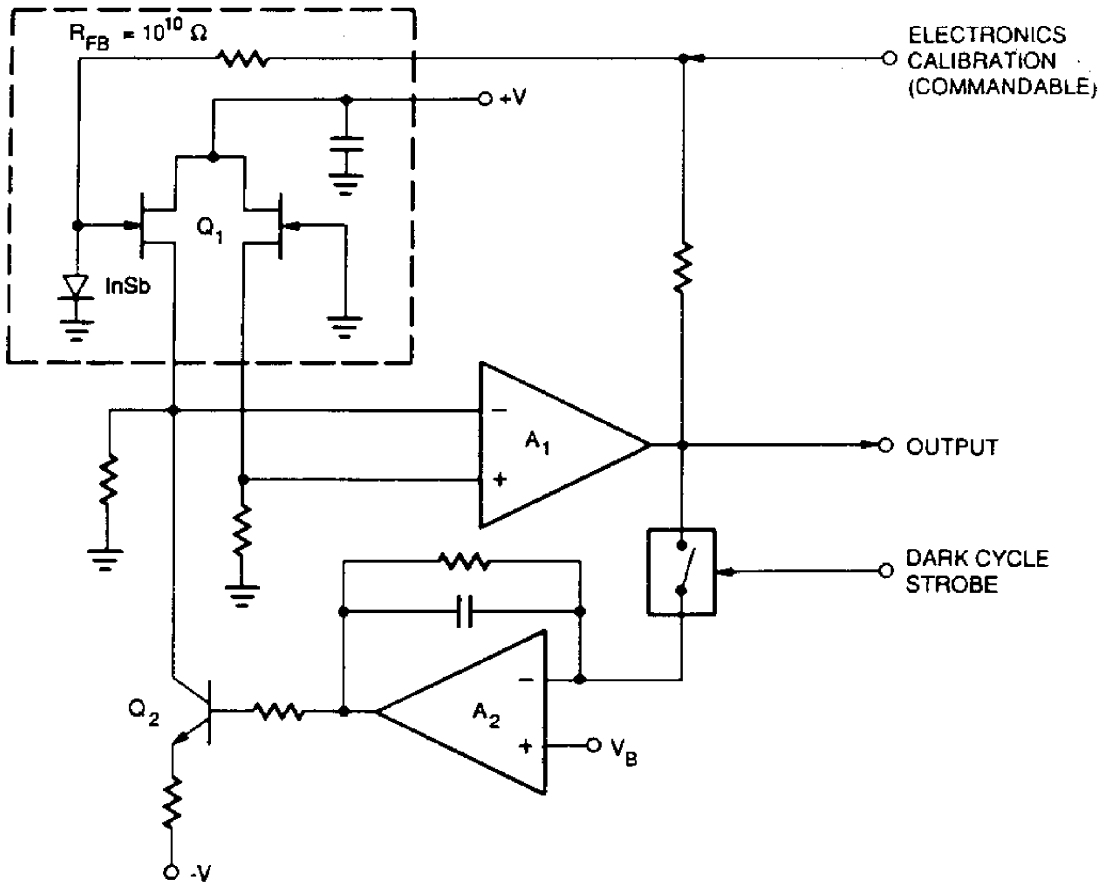

Fig. 8. Preamplifier and Autobias Circuitry.

The components (detectors, field effect input transistors, feedback resistors, and bypass capacitors) contained within the Focal Plane Assembly (FPA) are shown in the outlined rectangle in the upper left of the Figure. A differential source follower drives operational amplifier A1, which forms a transresistance amplifier using feedback resistor RFB. The output of this preamplifier feeds the remaining signal processing circuitry shown in Fig. 9. Automatic biasing of the detectors is accomplished by sampling the output of A1 during the dark portion of the chopper cycle; this signal is sampled and averaged using amplifier A2. The output of A2 controls the drain current of the input transistor, which controls its gate-source voltage VGS, and holds the bias of the InSb photodiode detector at zero bias voltage. With this zero bias condition, dark current changes due to changes in detector temperature remain small, yielding a large temperature operating range before amplifier saturation occurs. This bias condition also ensures detector linearity and minimizes detector noise.

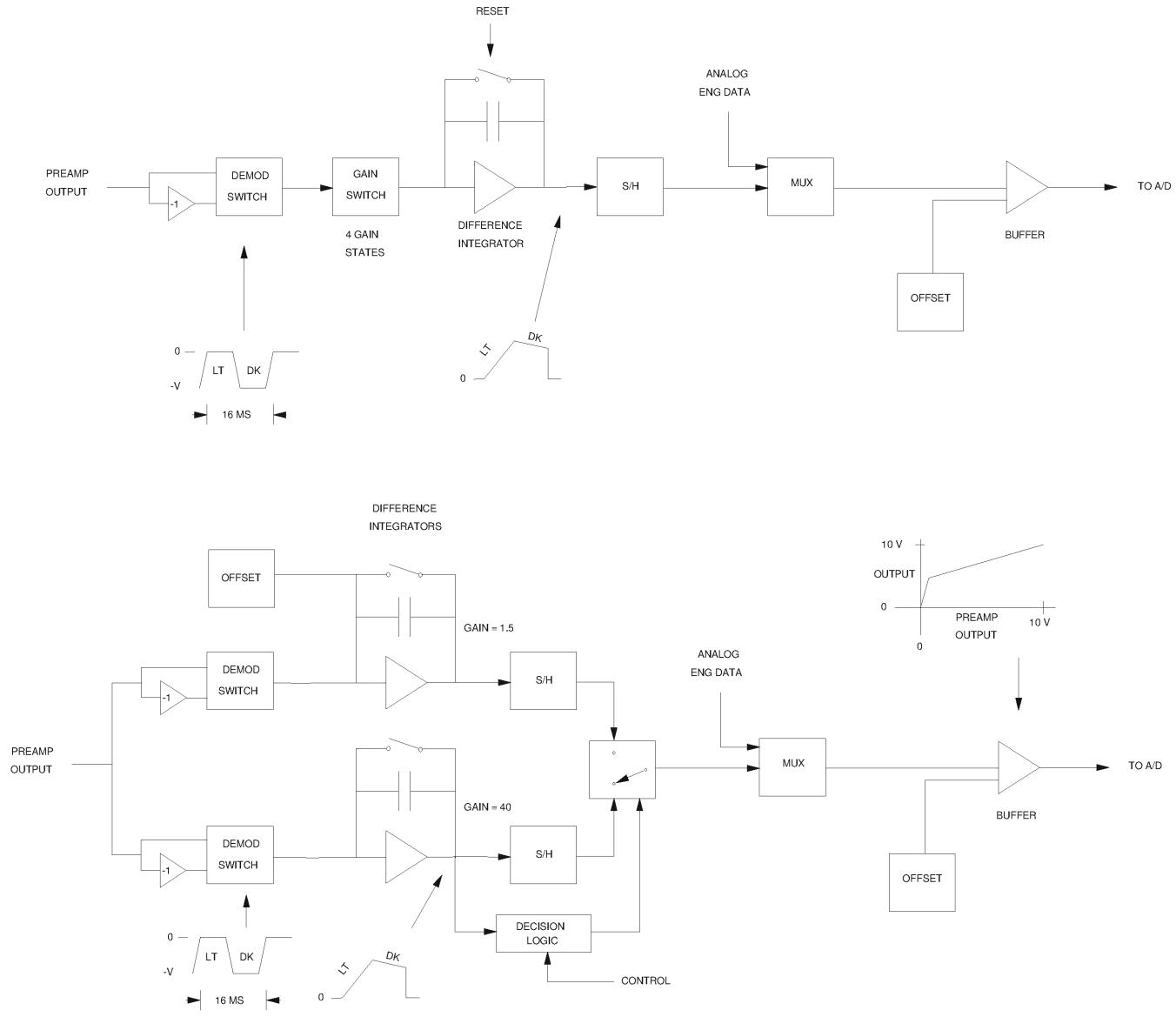

Fig. 9. Analog Signal Chain Electronics.

The upper diagram refers to detectors 1-14, termed the albedo channels, each of which has 4 commandable linear gain states. Preamplifier signals are synchronously demodulated and the current, which is determined by gain switched resistors, is integrated over one light/dark chopper cycle by the difference integrator. The integrated light-minus-dark signal is sampled at the end of each chopper cycle and stored by a sample-and-hold (S/H) circuit. It is then sequentially sampled by an analog multiplexer (MUX) andsent via an analog buffer to a 10-bit analog-to-digital converter (ADC). An offset is added in the buffer to ensure positive output values, > 0 DN. The signal path for each of the thermal channels, detectors 15-17, is shown below. The circuitry are similiar, but there are no commandable gain states. Instead, there are two independent paths, each with differing gains. The value sent to the MUX depends upon signal levels, yielding a large dynamic range.

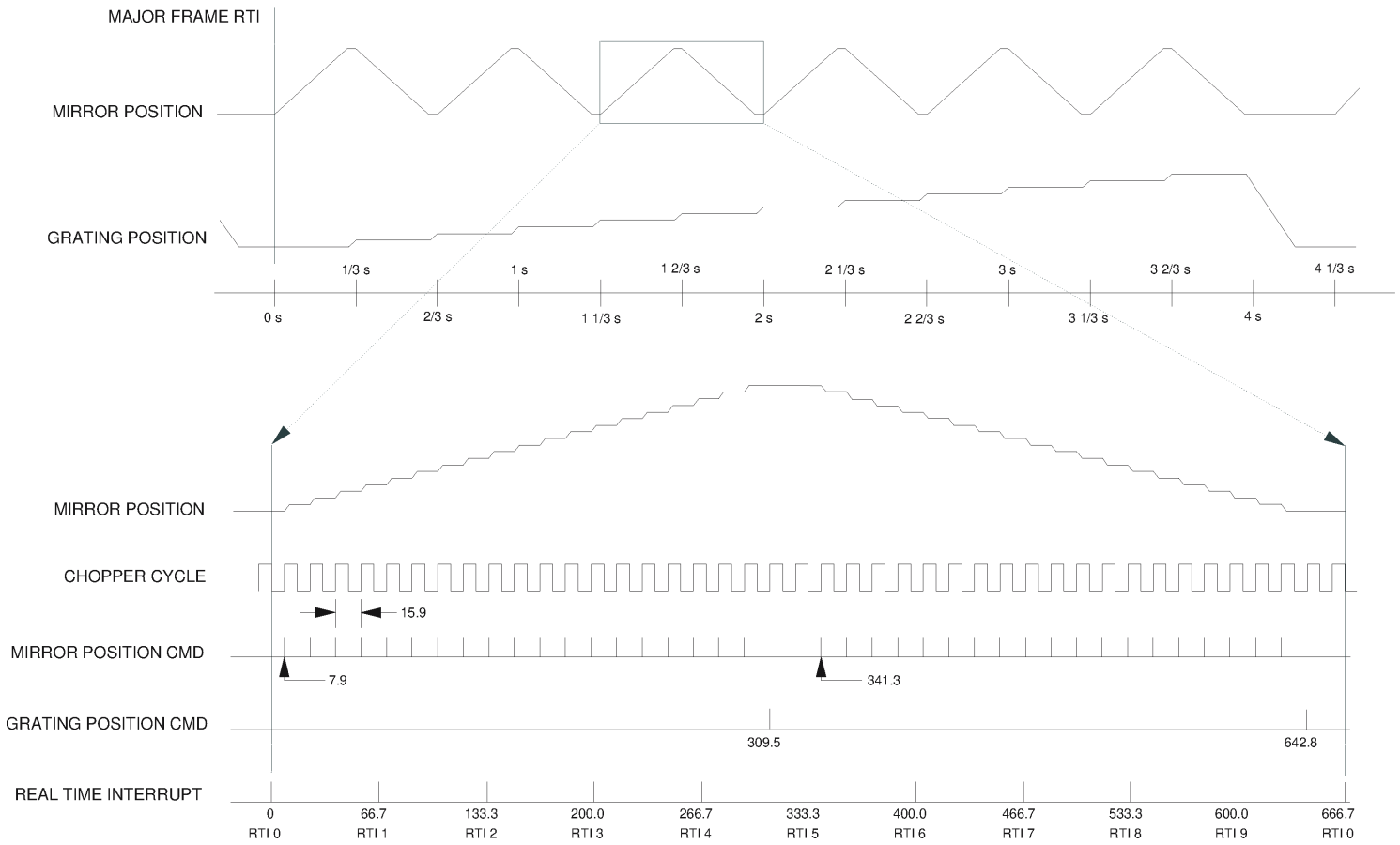

Fig. 10. Instrument Timing.

This timing diagram is representative of most NIMS modes, and particularly describes the the FULL MAP mode, which has 12 grating positions and a grating-flyback period, all occuring during a period of 4 1/3 sec (or 6 1/2 minor frames). During the grating flyback, the mirror

rests, so that the next spectral cycle has the same mirror motion for the same wavelengths. The mirror scan consists of 20 positions, each corresponding to a single chopper cycle of 1/63 sec duration. During the dark cycle of a chopper cycle, the mirror steps from one position to the next. At the end of a mirror scan, the mirror is stationary for one cycle, during which the grating steps to a new position.

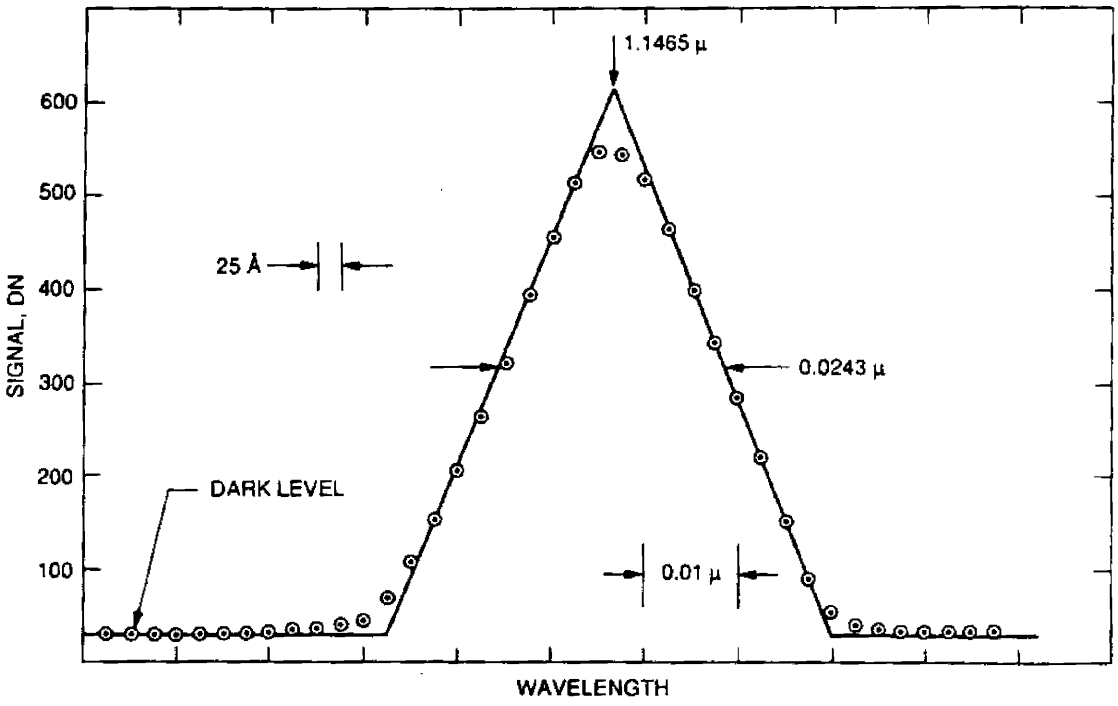

Fig. 11. Spectral Bandpass Response.

This Figure illustrates the spectral response of the instrument for a given detector and grating position, in this case Det. 3 and Position 13. An input monochromator, with a spectral bandpass of 25 A, was varied in wavelength to determine this instantaneous spectral response. The ideal response of the NIMS instrument is expected to be triangular, with a full-width-at-half-maximum (FWHM) bandwidth of 0.0250 microns. The experimental results are seen to be close to expectation. Roughly one half of the slight broadening is due to th finite bandwidth of the input monochromator, with the remainder arising from the finite spot sizes (abberations) of the NIMS spectrometer optics.

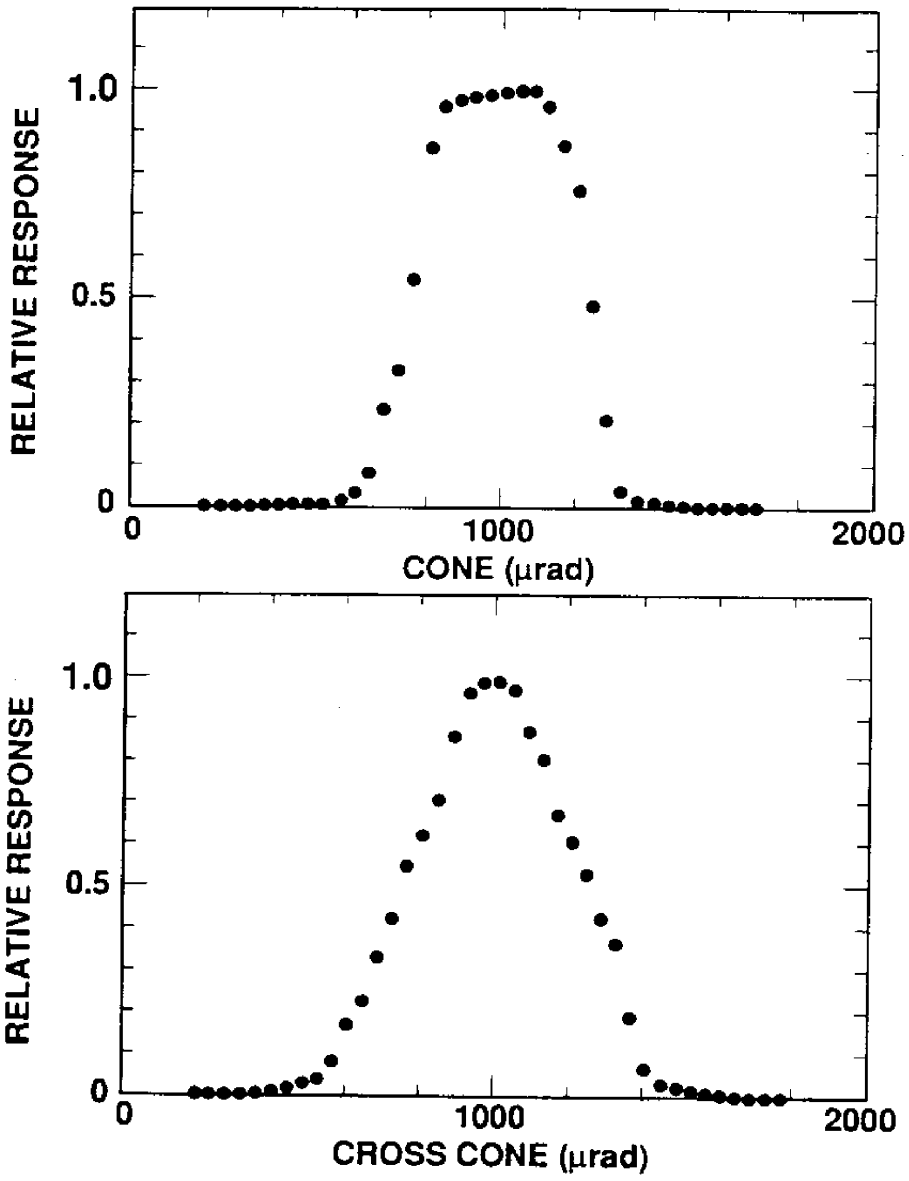

Fig. 12. Spatial Response.

This Figure illustrates the cone and cross-cone response of the NIMS instrument; see Fig. 2 for definitions. In the cone-angle direction (shown above), the response is rectangular, whereas the cross-cone response (below) is broadened by the natural astigmatism of the spectrometer.

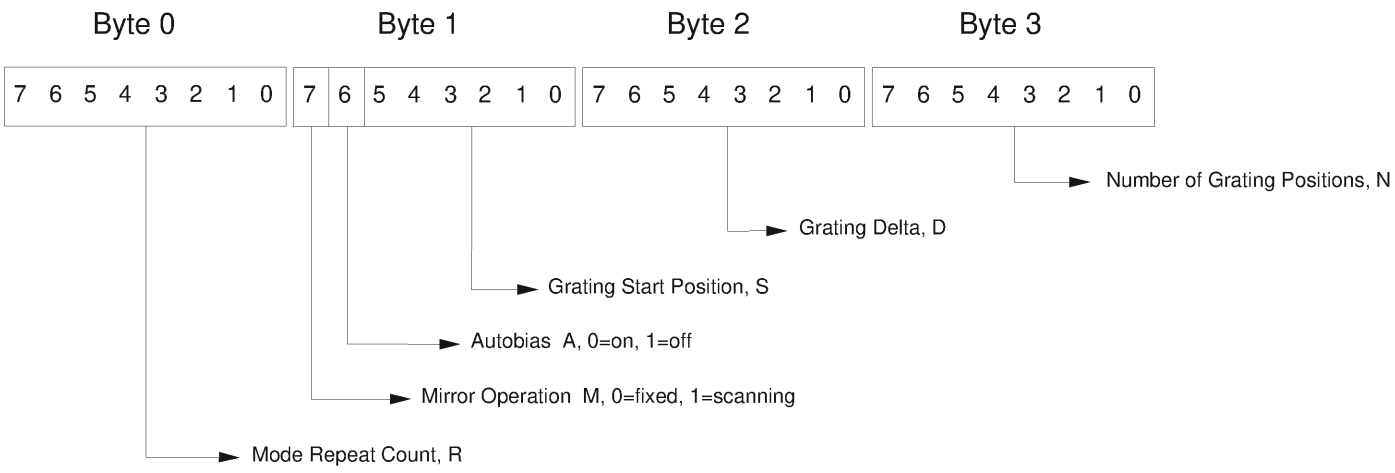

Fig. 13. Parameter Table Assignments.

Spectral modes are derived from the number of grating positions N, the increment between successive grating positions D, and the starting position of the grating, S. Spatial scanning is controlled by the mirror operation bit, M.

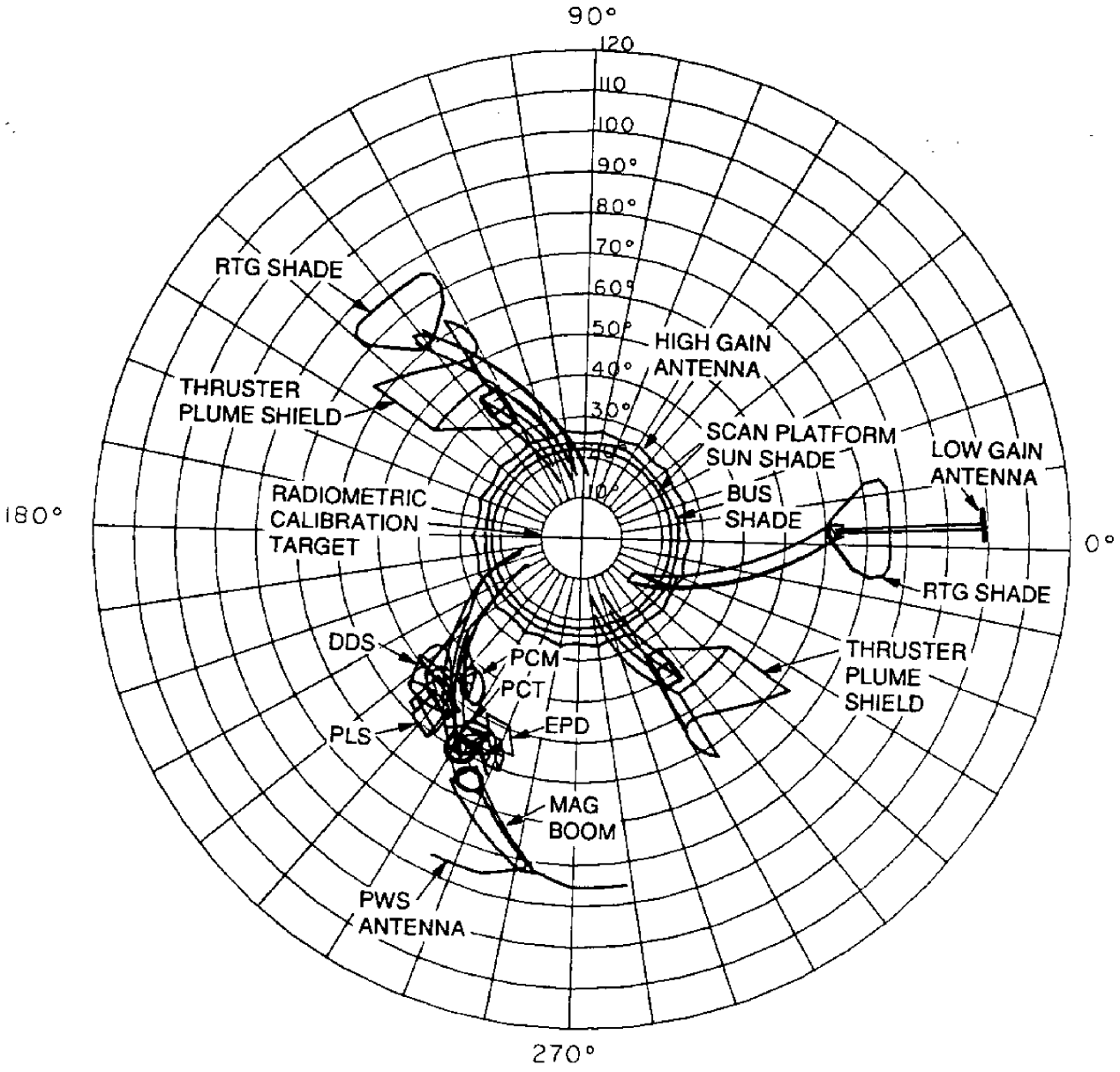

Fig. 14. Spacecraft Obscuration.

The obscuration and sun glint properties of the spacecraft, as seen by the NIMS instrument, are shown above. At the top (A) is a computer-generated plot showing the angular field which is completely clear of any obscuration within the NIMS field, taking into account the size of the telescope and the angular divergence of the field-of-view. In (B) we show an experimentally measured obscuration plot, obtained by NIMS during flight. It is a combination of sun glint, shown as red, and thermal emission, shown as green. Regions of relative warmth (~240 kelvins) which also include solar glint contributions appear as yellow. Note the bright Photometric Calibration Target (PCT), which is intentionally illuminated by the sun.